ACS OMEGA

http://pubs.acs.org/journal/acsodf

Article

Smartphone-Assisted Sensing of Trinitrotoluene by Optical Array

Rossella Santonocito, Nunzio Tuccitto, Valentina Cantaro, Antonino Biagio Carbonaro, Andrea Pappalardo, Valentina Greco, Valeria Buccilli, Pietro Maida, Davide Zavattaro, Gianfranco Sfuncia, Giuseppe Nicotra, Giuseppe Maccarrone, Antonino Gulino, Alessandro Giuffrida,* and Giuseppe Trusso Sfrazzetto*

Cite This: *ACS Omega* 2022, 7, 37122−37132

Read Online

ACCESS | Metrics & More | Article Recommendations | Supporting Information

ABSTRACT: Here we report the design and fabrication of an array-based sensor, containing functionalized Carbon Dots, Bodipy's and Naphthalimide probes, that shows high fluorescence emissions and sensitivity in the presence of low amounts of TNT explosive. In particular, we have fabricated the first sensor device based on an optical array for the detection of TNT in real samples by using a smartphone as detector. The possibility to use a common smartphone as detector leads to a prototype that can be also used in a real-life field application. The key benefit lies in the possibility of even a nonspecialist operator in the field to simply collect and send data (photos) to the trained artificial intelligence server for rapid diagnosis but also directly to the bomb disposal unit for expert evaluation. This new array sensor contains seven different fluorescent probes that are able to interact via noncovalent interactions with TNT. The interaction of each probe with TNT has been tested in solution by fluorescence titrations. The solid device has been tested in terms of selectivity and linearity toward TNT concentration. Tests performed with other explosives and other nitrogen-based analytes demonstrate the high selectivity for TNT molecules, thus supporting the reliability of this sensor. In addition, TNT can be detected in the range of 98 ng∼985 μg, with a clear different response of each probe to the different amounts of TNT.

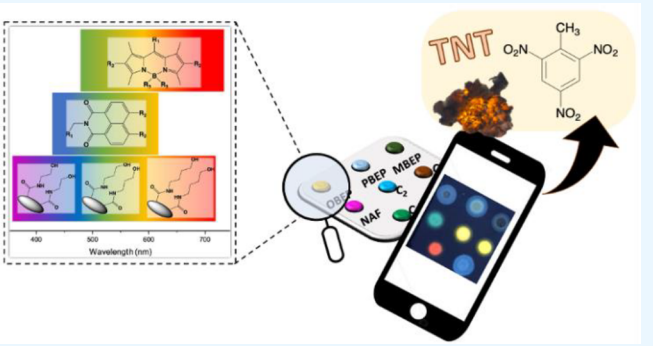

INTRODUCTION

Trinitrotoluene (Tritol or TNT), produced by the multistep nitration of toluene, is one of the most common explosives used in blasting charge assemblies of many different weapons.[1] In recent years, terrorist attacks using explosives have increased, and there is widespread construction of improvised explosive devices using explosive removed from the blasting charge of ammunition. For this reason, many efforts have been devoted to the detection and identification of explosive compounds.[2] In this context, numerous analytical techniques have been involved, such as gas and liquid chromatography,[3] ion mobility spectrometry,[4] surface-enhanced Raman spectroscopy,[5,6] and electrochemical detection,[7] just to name a few. However, these methods usually need complicated protocols and measurements, suitable for laboratory tests. Optical sensors can overcome these problems, thanks to the possibility to monitor changes in their optical properties in real time with cheap devices.[8−11] Array-based optical sensors exploit simultaneous interactions (physical adsorption or noncovalent interaction) of many probes with the target analyte, thus leading to a characteristic fingerprint, thus improving selectivity with respect to the classical molecular sensors[12] and avoiding false-positive responses. In particular, recently Peveler and co-workers reported an interesting system based on a multichannel quantum dots array able to detect TNT in ppb levels.[13] In addition, the use of a simple methodology to elaborate the array response is crucial for the applicability in real world. Smartphones, having a high-resolution digital camera and relevant computational capabilities for image data treatment, are practical ready-to-use "detectors"[14−18] that are able to give quantitative information on the optical/colorimetric changes of the probes into the array device. The smartphone approach is motivated by the fact that it can be used by a nonspecialized operator in the field, such as a regular police officer. Data acquired by a smartphone Internet connected can easily be sent to a centralized control system where trained artificial intelligence algorithms run for rapid analysis. In the presence of a positive result from the automatic test, the central system can alert the specialized bomb disposal

Received: May 12, 2022
Accepted: August 15, 2022
Published: October 14, 2022

https://doi.org/10.1021/acsomega.2c02958
ACS Omega 2022, 7, 37122−37132

units for an expert assessment and implement any necessary risk mitigation actions. Previously, smartphones have been successfully used as detectors to assess the presence of TNT in micromolar concentration by using PDMS polymer containing amines,[19] by an optical array using three probes (KI, creatinine, and aniline),[20] and by an impedance-based electrode containing TNT-specific peptides.[21]

Based on the above observations, we report here the design and fabrication of an array-based sensor, containing functionalized carbon dots (CDs), Bodipy's, and naphthalimide probes, selected for their high fluorescence emissions and sensitivity. In addition, their UV absorption and visible emission are ideal for their application in the sensor-array. Therefore, these functionalized probes have been properly synthesized and singly tested in solution for the TNT sensing. The final array device was tested for different TNT concentrations (from 10^{-2} to 10^{-6} M), and different responses were observed, depending on the explosive concentrations. The selectivity of the array was confirmed by using different explosives and competitors. Today, to the best of our knowledge, no examples on the use of a smartphone combined to an array device to detect TNT in real samples by fluorescence measurements have been reported. Moreover, the possibility to know in real time the nature of the explosive used in a terrorist attack will lead to an important intelligence source in the investigation.

RESULTS AND DISCUSSION

Array Design. The sensor array was designed to show emissions in a large visible range, upon a wide class of noncovalent interactions with the explosives (Figure 1). In particular, we have chosen three different classes of fluorescent sensitive probes: Bodipy's (OBEP, MBEP, and PBEP), naphthylamide (Naphthyl-Di-AE), and functionalized carbon dots (CDs-C_2-OH, CDs-C_3-OH, and CDs-C_4-OH).

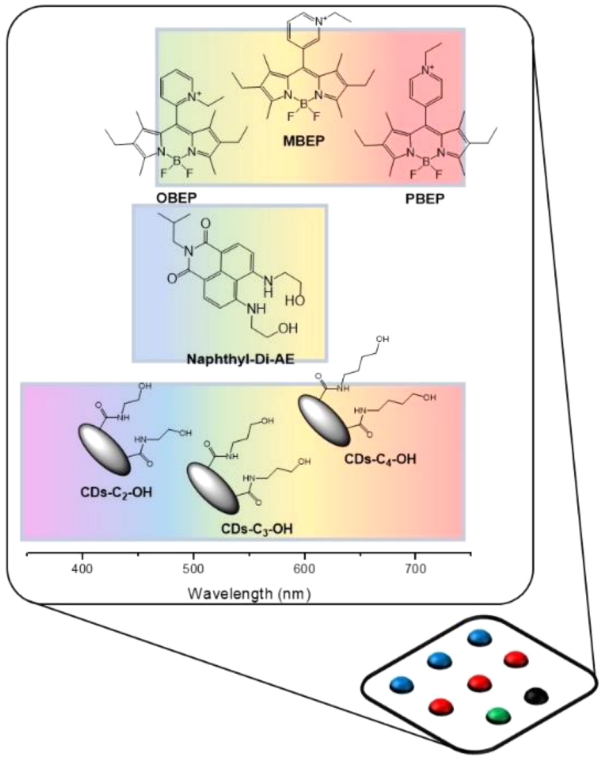

Figure 1. Molecular probes used in the array, relative emission ranges, and possible noncovalent interactions involved with the analytes.

Bodipy's, with an alkyl-pyridinium group (in ortho, meta, or para positions, respectively), lead to an emission in the 500−700 nm range, upon ion−dipole and dipole−dipole interactions with the present analyte.[22] Hydrogen bonds and $\pi-\pi$ interactions of Naphthyl-Di-AE with the analytes show emissions at shorter wavelengths, in the 450−600 nm range.[23] Carbon dots (CDs), due to their unique optical characteristics (such as photobleaching resistance, a wide absorption-emission range, modulable by covalent functionalization of the surface) show a wide range of emission wavelengths, depending on the external functionalization, their dimensions, and the excitation wavelength.[24−27] We have chosen three different CDs, with different aliphatic chain lengths. These CDs can establish hydrogen bonds, as well as $\pi-\pi$ interactions with the analytes. Syntheses of these probes were performed using simple synthetic protocols reported in the Supporting Information.

Molecular Sensing. Each molecular probe was tested in solution by fluorescence titrations. Figure 2 shows the normalized emission responses of each probe during the addition of TNT (Figure 2a−g) and the affinity values calculated (Figure 2h), assuming a 1:1 stoichiometry, as supported by Job's plots (see the Supporting Information). OBEP shows a large emission band centered at 540.2 nm, whose intensity increases upon the TNT addition (Figure 2d). MBEP shows an emission centered at 555.2 nm, whose intensity decreases during the addition of TNT (Figure 2e). TNT has also a quenching effect on PBEP emission (Figure 2f). Naphthyl-Di-AE shows an intense emission band, centered at 545.1 nm that in the presence of TNT suffers a strong emission quenching (Figure 2g).

Interaction of functionalized carbon dots with the explosives show a muted behavior: CDs-C_2-OH and CDs-C_4-OH show increased emission intensities upon the addition of TNT; on the contrary, the emission of CDs-C_3-OH is quenched by the explosive (Figure 2a−c).

Quenching of emission by photoinduced electron transfer (PET) is the main process involved in the TNT sensing.[29] This is due to the presence of nitro groups into the TNT scaffold, which render TNT an electro-deficient guest. However, recently some examples of nanosensors that are able to detect TNT by an increase of the emission, due to an aggregation phenomenon in solution induced by the presence of TNT, have been reported.[30,31] This phenomenon can explain the enhancement of the emission of CDs-C_2-OH and CDs-C_4-OH, while the PET mechanism with an enhancement of the emission can be invoked for OBEP. Further studies are in progress to demonstrate these hypotheses.

Sensing by Array. In a 4 × 4 cm of RP-18 thin layer, we casted on different surface portions 2 μL of the probe solutions (1 mg/mL of functionalized carbon nanoparticles in ethanol, 1 mM of Bodipy's and Naphthyl-Di-AE in $CHCl_3$). The size of each spot depends on the evaporation rate of the solvent. For this reason, the amount of solution dropped onto the silica surface was reduced a minimum. The solid device has been prepared by using silica gel (RP-18) as support, to reduce the interaction between the solid support and the probes or the analytes. The array was illuminated with a UV lamp (365 nm) in a dark chamber and the visible emission image was acquired with a smartphone (the experimental setup is reported in the Experimental Section). The as-prepared array was photo-

https://doi.org/10.1021/acsomega.2c02958
ACS Omega 2022, 7, 37122−37132

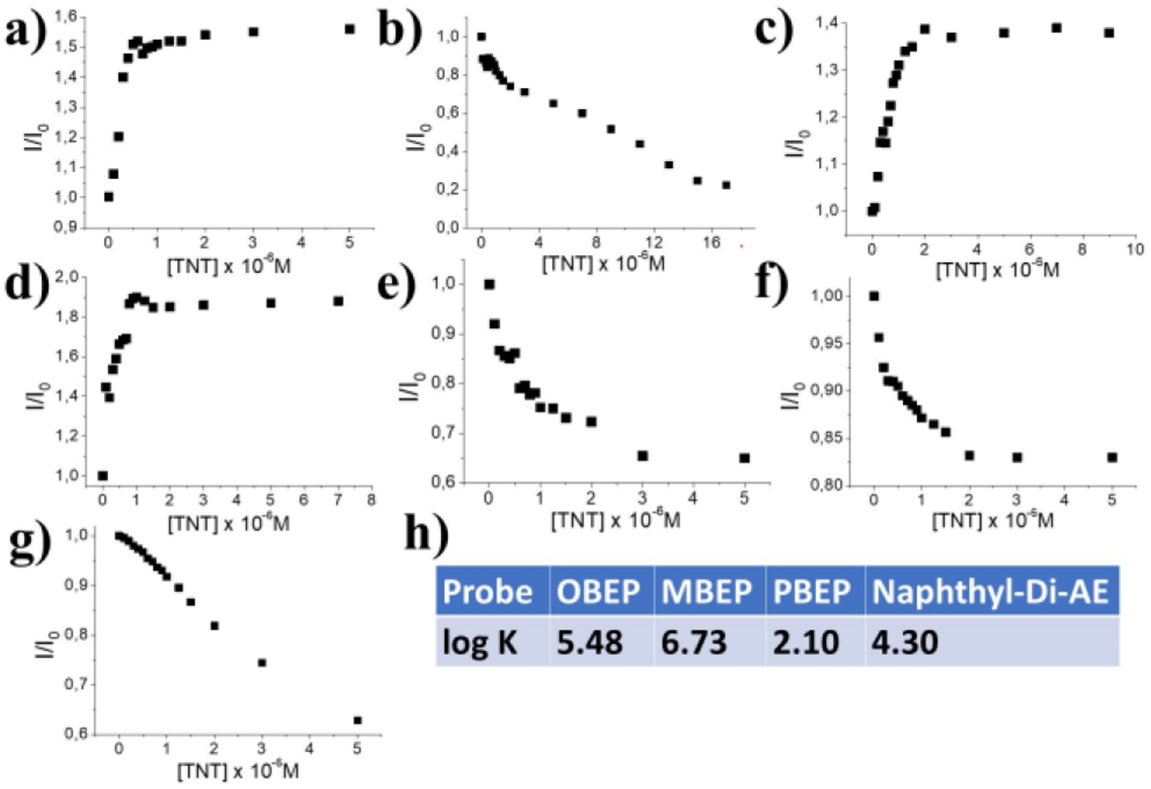

Figure 2. Normalized (I/I_0) fluorescence titrations of (a) CDs-C_2-OH, (b) CDs-C_3-OH, (c) CDs-C_4-OH, (d) OBEP, (e) MBEP, (f) PBEP, (g) Naphthyl-Di-AE with TNT, (h) affinity values calculated by HypSpec (version 1.1.33).[28] Probe concentrations were fixed at 1×10^{-6} M for molecular probes, 0.05 mg/mL for nanoparticles, while explosive amounts (μM) were added as described in the graphics.

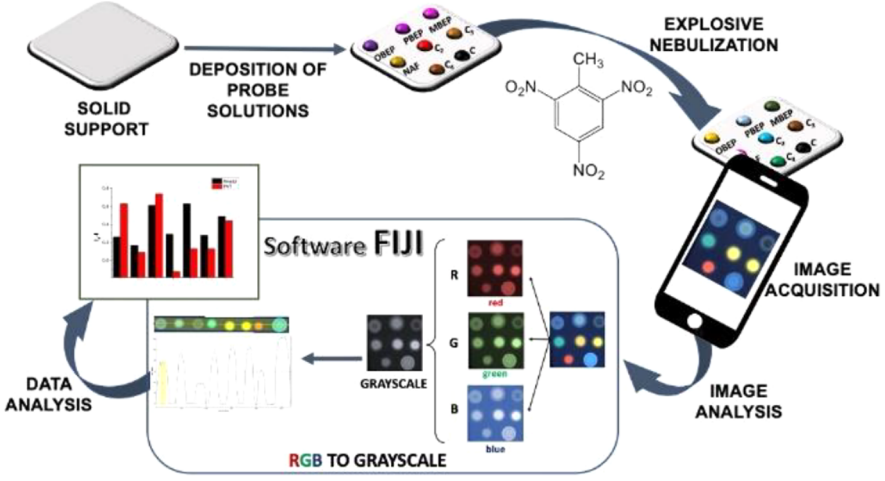

Figure 3. Schematic representation of the analysis process used in this work.

graphed by a smartphone (camera resolution 12 Mega pixel). Then, 10 nebulizations (having a total amount of 434 μL, average value verified after 10 different experiments) of a solution of the explosive (from 10^{-2} M to 10^{-6} M in water/CH_3CN 50/50 v/v ratio) was nebulized by a conical nebulizer onto the array (TLC sprayers). The amounts of nebulized TNT (98 ng~985 μg) have been calculated from the respective concentrations of the solutions of explosive and the volume nebulized. After evaporation on air at room temperature of the nebulized solvent, the array was further photographed, and the images before and after nebulization have been elaborated by Fiji.[32] In particular, images have been converted in RGB channel values, and converted into Gray scale value (G) by using the formula $G = (R_{value} + G_{value} + B_{value})/3$, thus obtaining a single value for each pixel. The emission intensities of this scale for each probe have been compared with the control (unfunctionalized carbon nanoparticles), and these normalized values (ratio between the intensity of the probe and the intensity of the control) have been reported. Gray channel values have been used to quantify TNT values, while *R*-, *G*-, and *B*- values have been used for selectivity tests. Each value is the average of three independent measures, also to reduce the experimental errors in the deposition of the probes onto the solid support. The resulting

https://doi.org/10.1021/acsomega.2c02958
ACS Omega 2022, 7, 37122−37132

values were tabulated for statistical treatment using Excel software (Microsoft 365).

Figure 3 summarizes the process involved in the explosive analysis by the obtained sensor array.

SELECTIVITY TESTS

To exclude false-positive responses, selectivity is a crucial parameter for a real practical sensor. In this context, array-based sensors are characterized by a higher selectivity with respect to classical molecular probes due to the possibility to have multiple responses by the combination of each sensor. Therefore, we validated the selectivity of our device measuring the response to other explosives (10 mM), in particular Amatol,[33] Premex, Anfo (ammonium nitrate fuel oil), dynamite,[34] and PEP,[35,36] and some common interfering analytes (10 mM), such as nitrobenzene, nitromethane, and ortho-dichloro benzene.

The results show a good possibility that the system could act as a sensor (see Supporting Information, Figure S12). For this purpose, a multivariate model based on PLS-DA was developed to recognize TNT from other explosives. Figure 4

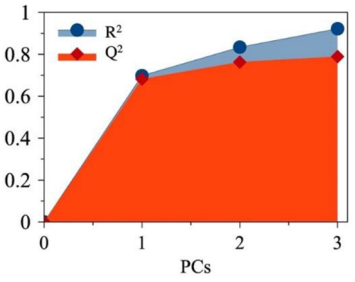

Figure 4. Cumulative R2Y and Q2Y of the classes TNT and no-TNT (other explosives and other interfering analytes, 10 mM in water/CH_3CN 50/50 v/v ratio) as a function of the components of the PLS-DA regression model (named as PCs).

displays the cumulative R^2 and Q^2 for both classes (TNT and no-TNT) after each component. These values represent how much of the differences between the two classes is explained by the model (R^2) and how well new observations can be classified into the proper class (Q^2).

Figure 5a reports the t1 vs t2, and Figure 5b shows the t1 vs t3 plots of the scores that can be interpreted as a window into the data matrix space. The observations are colored by classes. This shows how well the classes are separated as well as the presence of outliers (observations outside the confidence interval). Only one sample of TNT is outside the Hotelling ellipse and only one no-TNT sample is close to the TNT class cluster, indicating a very good classification capability of the model. Figure 5c shows the X- and Y-weights (w*c) of the first PLS component against the second one and Figure 5d shows of the first against the third. These plot the X matrix variables in black and the two classes in red as dummy variables. The variables closest to each group are those that correlate positively the most with each group. In particular, the most correlating variables with TNT class are the signals related to the R-channel of CDs-C_2-OH, CDs-C_3-OH, PBEP and the G-channel of MBEP.

Table S1 (see the Supporting Information) shows the complete list of the other explosives and interferents that we here defined as "no TNT", each associated with the Euclidean distance with center of maximum density of "TNT" samples in the t1-t2-t3 space, having coordinate (1.77;0.77;0.48) as reported in Figure S11 (see the Supporting Information). This value represents an estimation of the difficulty to discriminate TNT from the other analytes, revealing that dynamite is the explosive that shows a closer response with respect to TNT and which, therefore, could more easily be mistaken.

Table 1 shows the confusion matrix regarding the classification/misclassification of TNT compared with other explosives. The results are outstanding, and in all cases, TNT is recognized as belonging to its class. In 4% of the cases the model was unable to recognize a sample of no-TNT class as belonging to one of the two classes, but still did not incorrectly assign it to the class of TNT. These results allow us to state that the recognition method is certainly capable if properly trained.

Quantification of TNT. Then we tested the possibility to quantify TNT in solutions with different concentrations, from 10^{-2} M to 10^{-6} M (corresponding to 985 μg−98 ng amounts, respectively). In particular, the appropriate solution of TNT has been nebulized onto the array to test its response. After explosive nebulization, the array was dried in air for 30 s, and images have been acquired. As previously described, grayscale channel values were used to quantify the amount of nebulized TNT.

In particular, Figure 6 shows the emission change of each probe upon the TNT exposure, from 10^{-2} M to 10^{-6} M, showing that different TNT concentrations lead to different emission changes of each probe of the array, thus leading to the possibility to discriminate TNT in this range. Notably, the results shown in Figure 6 have been obtained by three different experiments, supporting the good repeatability of the array response.

In attempting to provide quantitative information, we analyzed fluorescence intensity changes of arrays subjected to different concentrations of analytes, by applying a multivariate descriptor calculated according to the following equation:

$$D = \sum_{i=j}^{n} \left[\frac{1}{m} \sum_{j=1}^{m} (\Delta I_j - \overline{\Delta I})^2 \right]^{1/2} \quad (1)$$

where n is the number of sensors in each array, ΔI is the detected variation in fluorescence intensity acquired at the j-th replica, and $\overline{\Delta I}$ is the average of the fluorescence changes of the m replicas acquired for each i-th sensor.

This equation arises from the necessity to use a quantitative descriptor that allows the rapid determination of the TNT concentration identified by the proposed agile method without performing specific analytical tests. Its derivation is based on a detailed study of signals. It is based on the evaluation of the correlation between the variation of fluorescence intensities upon the TNT concentration changes.

Figure 7 shows the D value as a function of the TNT concentration, nebulized onto the fluorescent array. The obtained trends are roughly linear, and the present analytical approach has, therefore, some potential also from a quantitative point of view.

These results show a linearity of TNT detection comparable with other sensors for TNT, in particular by exploiting carbon nanoparticles, in which the linearity of the emission response and the limit of detection are in micromolar[37,38] or nanomolar[39,40] concentrations. In this context, Zhan and co-

https://doi.org/10.1021/acsomega.2c02958
ACS Omega 2022, 7, 37122−37132

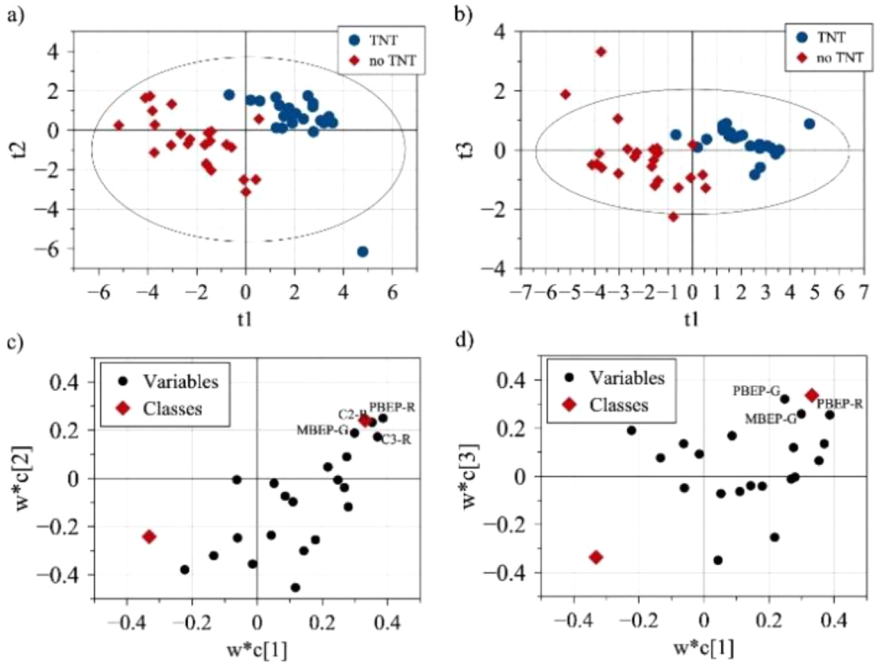

Figure 5. PLS-DA model results. (a) Scores plot t1 vs t2, (b) t1 vs t3 of the binary PLS-DA model. Blue dots refer to TNT tests, and red dots represent no-TNT samples class; (c) weights' plot related to the first two principal components reporting variables of X matrix (black dots) and Y matrix (red dots as dummy variables representing both classes); (d) weights' plot of first and third components.

Table 1. Confusion Matrix of PLS-DA Classification

confusion matrix	class 1 TNT	class 2no-TNT	no class	class 1 and 2
class 1 TNT	100%	0	0	0
class 2 no-TNT	0	96%	4%	0

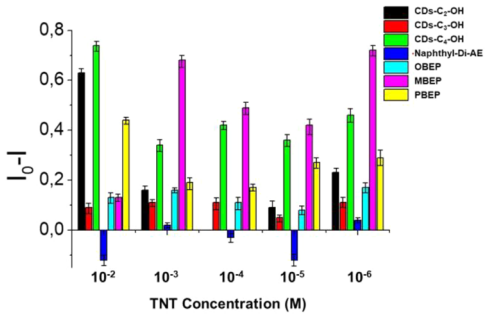

Figure 6. Normalized emission responses of gray channel (I_0−I, where I_0 and I are the gray channel emission values and relative standard deviation before and after exposure to explosive, respectively) of the probes upon the exposure to 10^{-2} M (985 μg), 10^{-3} M (98.5 μg), 10^{-4} M (9.85 μg), 10^{-5} M (985 ng), and 10^{-6} M (98 ng) of TNT in H_2O/CH_3CN 50/50).

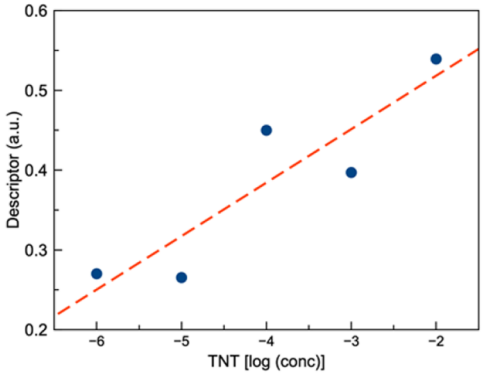

Figure 7. Trend of the multivariate descriptor calculated according to equation reported above as a function of the molar concentration (log scale) of TNT.

workers reported an interesting nanosensor for the detection of TNT in nanomolar concentrations, by using reusable magnetic core−shell nanoparticles.[41] Comparing our array device with respect to these systems, our prototype shows the possibility to be simply used with a smartphone as fluorescence detector. In addition, as previously described, a smartphone has already been used for the detection of TNT by using an array device by Paixão and co-workers,[20] who obtained the detection of the explosive in the range of micrograms with a colorimetric response. In the present study, the use of fluorescence leads to a higher sensibility, detecting nanograms of TNT.

We noted that fluorescent probes show, in general, different behavior from solution to solid-state studies. This phenomenon is not unusual, probably due to different aggregation phenomena that occur from the solution to solid phases.[24,42]

To demonstrate the suitability of this device in real sample analysis, we tested the ability to detect TNT in a mixture with agricultural soil (to simulate the presence of TNT in a land) and food flour (in some terroristic scenarios, the explosives are smuggled into food supplies). In particular, we mixed 100 mg of TNT with 500 g of the real matrix (soil or flour), thus obtaining a sample containing the 0.02% of TNT. Then, we sampled 1 g of this mixture and extracted the organic component, including TNT, with 20 mL of H_2O/CH_3CN 50/50. The solid phase was filtered, and the solution was nebulized onto the array. The response of each probe is unaltered with respect to the exposure to pure TNT, in particular to the array exposed to a 10^{-5} M solution, thus suggesting the possibility to use the prototype in the real field

https://doi.org/10.1021/acsomega.2c02958
ACS Omega 2022, 7, 37122−37132

(see the Supporting Information). The good match between the amount of TNT detected in the solid matrix and the amount introduced experimentally supports the reliability of the array.

CONCLUSIONS

In this study, we reported the realization of a new array sensor, based on 7 different fluorescent probes that are able to detect TNT in a 10^{-2} M−10^{-6} M concentration range. Each probe has been tested in solution as a sensor for the detection of TNT. The final array, under UV lamp illumination (365 nm), can be used in combination with a common smartphone leading to a qualitative and quantitative information about the presence of TNT by image elaboration. Selectivity tests were successfully performed by using common explosives, such as Amatol, Premex, Anfo (ammonium nitrate fuel oil), dynamite and PEP, and other competitors, such as nitromethane, nitrobenzene, and ortho-dichloro benzene, demonstrating the possibility to discriminate the presence of TNT. We are working to (*i*) optimize the deposition method of the probes onto the solid support (also by an inkjet-printer), to obtain a solid device having uniform probe spots; (*ii*) to optimize the portability of the system, by using commercial UV lamps and optical fibers as detector; and (*iii*) to automate the analysis by an application for smartphone, exploiting a multivariate analysis approach to obtain a rapid response on the presence of the explosives. This prototype paves the way for the realization of new array-based sensors, able to exploit noncovalent interactions in the sensing of important and dangerous analytes. Being a process based on detection with a smartphone connected to the Internet, the device can easily be integrated into an action plan where a nonexpert operator working in the field sends the data to an artificial intelligence system that can make a rapid diagnosis and alert, if necessary, the expert bomb disposal unit.

EXPERIMENTAL SECTION

General Experimental Methods. The NMR experiments were carried out at 27 °C on a Varian UNITY Inova 500 MHz spectrometer (^{1}H at 499.88 MHz, ^{13}C NMR at 125.7 MHz) equipped with a pulse field gradient module (Z axis) and a tunable 5 mm Varian inverse detection probe (ID-PFG). ESI mass spectra were acquired on a API 2000- ABSciex using CH_3CN or CH_3OH (positive or negative ion mode). Synthesis and characterization of Naphthyl-Di-AE was performed following a published synthetic protocol.[23]

In particular, nanoparticles as synthesized have an elliptical shape with average dimensions between 15 and 20 nm and a multilayer graphitic structure. The functional groups on the surface, as well as the covalent functionalization, have been identified and verified by extensive XPS analysis (vide infra). Due to the relation of sensing properties with the size and degree of functionalization of a carbon nanoparticle, the reproducibility of these nanoparticles leads to the realization of sensors with solid optical characteristics.

A JASCO V-560 UV−vis spectrophotometer equipped with a 1 cm path-length cell was used for the UV−vis measurements (resolution 0.1 nm). Luminescence measurements were carried out using a Cary Eclipse Fluorescence spectrophotometer with resolution of 0.5 nm, at room temperature. The emission was recorded at 90° with respect to the exciting line beam using 5:5 slit-widths for all measurements. All chemicals were reagent grade and were used without further purification. X-ray photoelectron spectra (XPS) were measured at a 45° takeoff angle relative to the surface normal with a PHI 5600 Multi Technique System (base pressure of the main chamber 3 × 10−8 Pa). Samples were excited with the Al Kα X-ray radiation using a pass energy of 5.85 eV. Structures due to the Kα satellite radiations were subtracted from the spectra prior to data processing. Spectra calibration was achieved by fixing the C 1s signal at 285.0 eV. The instrumental energy resolution was ≤0.5 eV. The XPS peak intensities were obtained after Shirley background removal. The atomic concentration analysis was performed by taking into account the relevant atomic sensitivity factors. The fittings of the C 1s, N 1s, and O 1s XP spectra were carried out using Gaussian envelopes after subtraction of the background until there was the highest possible correlation between the experimental spectrum and the theoretical profile. The residual or agreement factor R, defined by $R = [\sum(F_{obs} - F_{calc})^2/\sum (F_{obs})^2]^{1/2}$, after minimization of the function $\sum(F_{obs} - F_{calc})^2$, converged to the value of 0.03. Samples for XPS measurement were deposited on silicon substrates.

Explosive samples were received by RIS (Reparto Carabinieri Investigazioni Scientifiche − Messina) after a confiscation.

Procedure for Fluorescence Titrations. Two mother solutions of probe and explosive (1.0×10^{-3} M) in H_2O/CH_3CN (50/50 v/v) were prepared. This mixture allowed the full solubilization of the explosive samples. From these, different solutions with different receptor/guest ratios were prepared (in cuvette, probe concentration was fixed at 1×10^{-6} M, while explosives were added in a concentration range from 0 to 1.8×10^{-5} M), and emission spectra were recorded at 25 °C. The apparent binding affinities of probes with the explosives were estimated using HypSpec (version 1.1.33),[28] a software designed to extract equilibrium constants from potentiometric and/or spectrophotometric titration data. HypSpec starts with an assumed complex formation scheme and uses a least-squares approach to derive the spectra of the complexes and the stability constants. χ^2 test (chi-square) was applied, where the residuals follow a normal distribution (for a distribution approximately normal, the χ^2 test value is around 12 or less). In all of the cases, $\chi^2 \leq 10$ were found, as obtained by three independent measurements sets.

Determination of Stoichiometry. The stoichiometry of the complexes was investigated by the Job's plot method, using spectrophotometric measurements. The samples were prepared by mixing equimolecular stock solutions (1.0×10^{-3} M) of the appropriate probe and explosive to cover the whole range of molar fractions, keeping constant the total concentration (1×10^{-5} M). The changes in absorbance compared to uncomplexed receptor species ($\Delta A \times \chi^{-1}$) were calculated and reported versus the receptor mole fraction (χ). These plots show a maximum at 0.5 mole fraction of receptor, thus suggesting its 1:1 complex formation.

Procedure for Sensing by Array: Experimental Setup. The UV−vis lamp power 6 W, and the excitation wavelength was 365 nm. The position of the array device into the dark chamber can be modified, due to the presence of the control probe. In fact, the possible variations of the irradiation are normalized by the comparison with the control. The array device is located at 20 cm from the smartphone and UV source. The dark chamber used is reported in Figure 8.

https://doi.org/10.1021/acsomega.2c02958
ACS Omega 2022, 7, 37122−37132

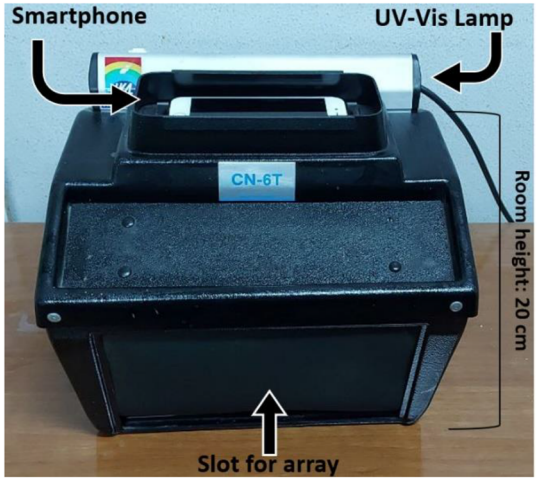

Figure 8. Dark chamber used in this work.

Synthesis of Probes. Bodipy probes have been synthesized following the reaction pathway, as shown in Scheme 1. In particular, starting from kryptopyrrole, in the presence of the appropriate carboxy-aldehyde, with a catalytic amount of trifluoroacedic acid, and after addition of DDQ (2,3-dichloro-5,6-dicyano-1,4-benzoquinone), triethylamine, and boron trifluoride, the corresponding fluorophore was obtained (OBP, MBP and PBP, respectively). Reaction of these compounds with a large excess of iodoethane leads to the desired probes. Naphthyl-Di-AE has been synthesized starting from Br-NO_2-anhydride 1 which in the presence of isobuthylamine leads to the diimide derivative 2. The reaction of this compound with a large excess of ethanolamine (10 equiv) at high temperature leads to Naphthyl-Di-AE (Scheme 2).

Scheme 1. Synthetic Pathway for the Synthesis of Bodipy Probes[a]

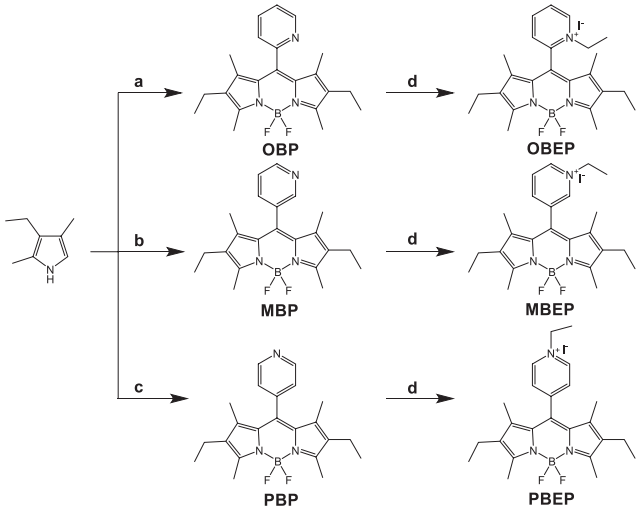

[a]Reagents and conditions: (a) 2-Pyridinecarboxaldehyde, TFA, DDQ, Et_3N, $BF_3(OEt)_2$, CH_2Cl_2, r.t.; (b) 3-Pyridinecarboxaldehyde, TFA, DDQ, Et_3N, $BF_3(OEt)_2$, CH_2Cl_2, r.t.; (c) 4-Pyridinecarboxaldehyde, TFA, DDQ, Et_3N, $BF_3(OEt)_2$, CH_2Cl_2, r.t.; (d) Iodoethane, CH_3CN, 50°C.

Synthesis and Functionalization of CDs. Carbon nanoparticles were prepared starting from citric acid and following a reported literature procedure.[43] In a typical procedure for synthesis of CDs, 21 g of citric acid was put into a 500 mL beaker and heated at 215 °C. About 10 min later, salts were liquefied obtaining a pale-yellow liquid, which turned into dark in 15 min, implying the formation of CDs. The obtained liquid was cooled down to room temperature, and 200 mL of a 0.25 M aqueous solution of NaOH was added dropwise under vigorous stirring. The solution was centrifuged at 15 000 rpm for 2 h at 3 °C, and the supernatant solution was dialyzed for 24 h using a tube having a 11.000 Da cutoff. The dialyzed aliquot was freeze-dried and used for the subsequent covalent functionalization. This is reported in Scheme 3 and was carried out by exploiting the reactivity of the carboxylic groups of their external shell. In particular, 100 mg of CDs was introduced into a round-bottom flask, saturated with nitrogen, and 20 mL of thionyl chloride and 500 μL of pyridine were added. The mixture was heated at 50 °C overnight; then 1 mL of the corresponding amino alcohol was added, and the reaction mixture was stirred for 3 days at 50 °C. Then, the

Scheme 2. Synthesis of Naphthyl-Di-AE[a]

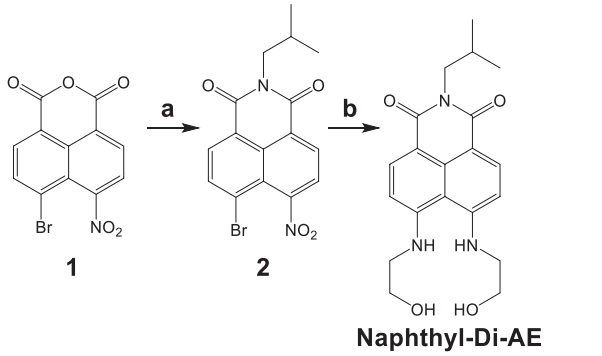

[a]Reagents and conditions: (a) isobuthylamine, ethanol, 50 °C, 18 h, 56%; (b) ethanolamine, 2-methoxyethanol, reflux, 36 h, 47%.

Scheme 3. Synthesis of Functionalized Carbon Nanoparticles[a]

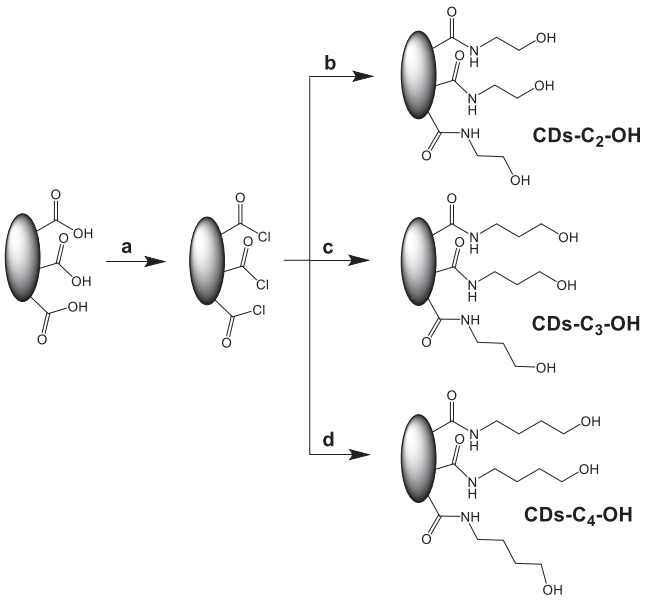

[a]Reagents and conditions: (a) $SOCl_2$, pyridine, 50°C, 18 h; (b) ethanolamine, reflux, 48 h; (c) propanolamine, reflux, 48 h; (d) butanolamine, reflux, 48 h.

https://doi.org/10.1021/acsomega.2c02958
ACS Omega 2022, 7, 37122−37132

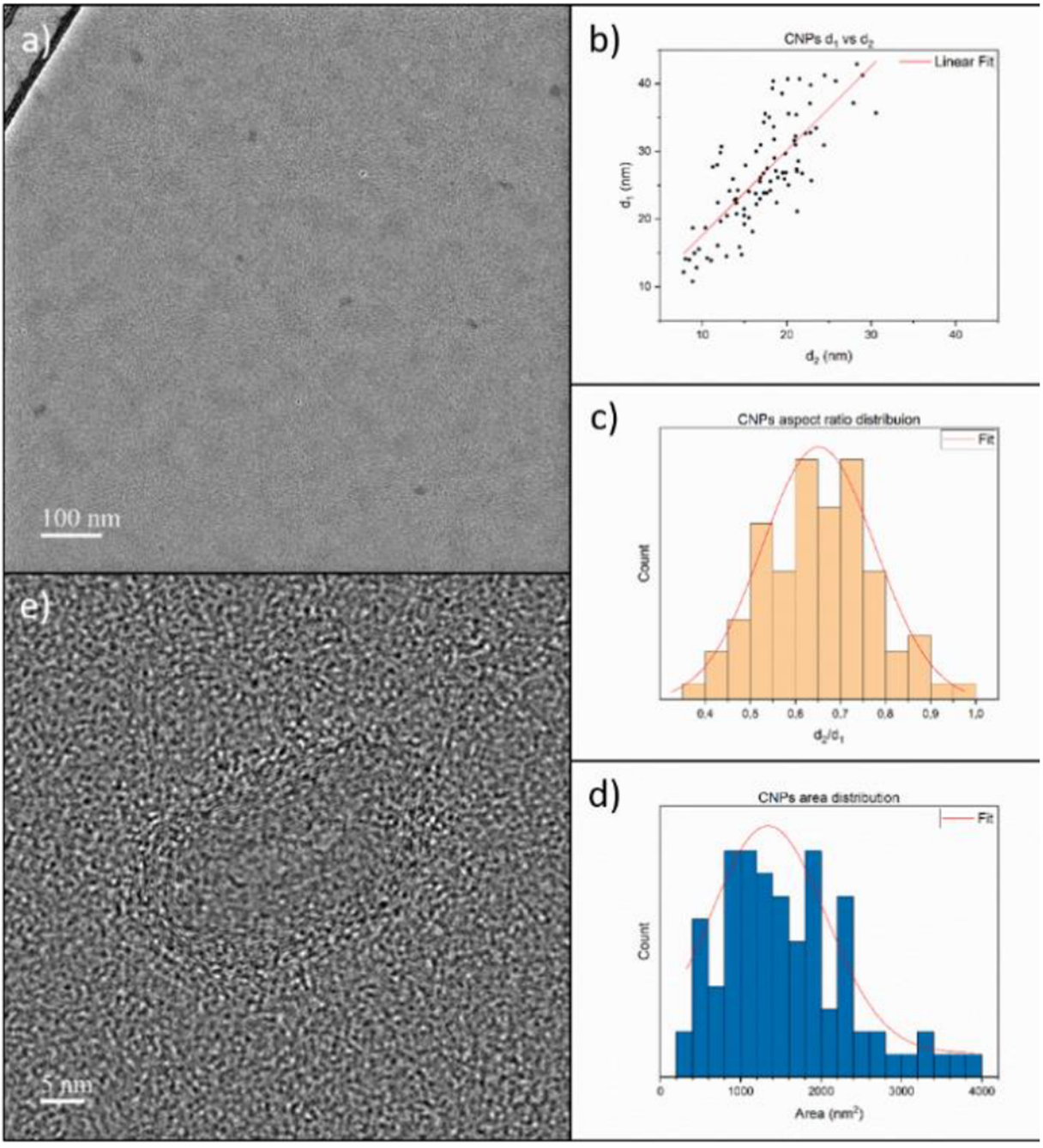

Figure 9. (a) TEM imaging of carbon nanoparticles showing their elliptical shape. (b) Correlation between major axis (d_1) and minor axis (d_2) of CDs. (c) Distribution of the aspect ratio. (d) Distribution of CDs' area. (e) HR-TEM of a CD showing more than 10 graphitic layers with superelliptical shape.

excess of thionyl chloride was removed under reduced pressure, and the crude compound was washed with H_2O and CH_2Cl_2. The desired CDs were purified by dialysis (cutoff 11 000 Da). XPS analysis supports the CNs covalent functionalization; in particular, the peaks at 285.7 and 286.9 and 288.6 eV are due to the C-N and C-OH and -OC-NH- groups, respectively, and the presence of some of these signals confirms the covalent functionalization of the nanoparticles with the amino alcohol (see Figure S1−S2).

Transmission electron microscopy (TEM) imaging of carbon nanoparticles was performed using a JEOL JEM-ARM200F and a cold field emission scanning transmission electron microscope (S/TEM) with probe aberration correction. Images were acquired at 200 kV using a Gatan Orius SC200D Charged Coupled Device (CCD) 4MP Camera. For TEM sample preparation, 10 μL of a CDs acqueous dispersion was dropcasted on a TEM copper grid having a continuous ultrathin (<3 nm) carbon film supported by a lacey carbon film. TEM imaging showed well-dispersed CDs (Figure 9a), having a superelliptical shape plotted by assuming exponents equal to 1 and 10 respectively on the Lamé curve (Figure 9e). Typical lengths of the major axis (d_1) and minor axis (d_2) go roughly from 10 to 45 nm (Figure 9b), and the average aspect ratio, calculated as d_2/d_1, is 0.65 (Figure

https://doi.org/10.1021/acsomega.2c02958
ACS Omega 2022, 7, 37122−37132

9c). CDs areas, calculated assuming a regular elliptical shape as $d_1*d_2*\pi$, show a distribution peak at 1340 nm^2 (Figure 9d). High-resolution (HR) TEM imaging highlighted the presence of several (>10) graphitic layers forming the structure of CDs (Figure 9e).

PLS-DA Classification. The image in the visible spectrum of the array was acquired in a dark box equipped with an ultraviolet source (UVC) for the excitation of the fluorescent probes constituting the sensitive elements of the colorimetric array. The image was captured by the smartphone camera and was referred to as the "background image". After exposure of the array to the analytes, a new image is reacquired under the same conditions and was referred to as the "sample image".

The red, green, and blue (RGB) color intensity values of all the pixels of the array spots were extracted by means of scripts developed by the authors based on the open-source library named "Python Imaging Library". For both images, the average RGB values on all pixels of each spot were calculated and then the differences between the average color values of the sensors before and after exposure to the analyte were calculated. The values of ΔR, ΔG and ΔB were used as analytical data to provide the color difference map (CDM). Therefore, for each sensor spot, 3 numbers were obtained corresponding to the differences in the mean values of the red, green, and blue color. Consequently, for each sample, a response data vector of size 7 sensors × 3 color elements is collected and saved as a "comma separated value". This vector contained both negative and positive values. Twenty-three TNT recognition tests (called TNT class) were replicated. Twenty-four samples related to the sensing of other explosive compounds (called no-TNT class) were acquired for the purpose of evaluating the discriminatory capabilities of the method. A matrix consisting of 21 variables for 47 objects was then assembled and saved as a "comma separated value". The matrix was used for the construction of the recognition model of the two classes based on the methodology called PLS Discriminant Analysis for binary classification. Simca-P11 (Umetrics) was used for this purpose.

■ ASSOCIATED CONTENT

Supporting Information

The Supporting Information is available free of charge at https://pubs.acs.org/doi/10.1021/acsomega.2c02958.

Detailed experimental procedures, XPS analysis, fluorescence measurements, HypSpec plots (PDF)

■ AUTHOR INFORMATION

Corresponding Authors

Alessandro Giuffrida − *Department of Chemical Sciences, University of Catania, 95100 Catania, Italy*; Email: agiuffri@unict.it

Giuseppe Trusso Sfrazzetto − *Department of Chemical Sciences, University of Catania, 95100 Catania, Italy; National Interuniversity Consortium for Materials Science and Technology (I.N.S.T.M.), Research Unit of Catania, 95125 Catania, Italy;* orcid.org/0000-0003-1584-5869; Email: giuseppe.trusso@unict.it

Authors

Rossella Santonocito − *Department of Chemical Sciences, University of Catania, 95100 Catania, Italy*

Nunzio Tuccitto − *Department of Chemical Sciences, University of Catania, 95100 Catania, Italy; Laboratory for Molecular Surfaces and Nanotechnology, CSGI, 95125 Catania, Italy;* orcid.org/0000-0003-4129-0406

Valentina Cantaro − *Department of Chemical Sciences, University of Catania, 95100 Catania, Italy*

Antonino Biagio Carbonaro − *Department of Chemical Sciences, University of Catania, 95100 Catania, Italy*

Andrea Pappalardo − *Department of Chemical Sciences, University of Catania, 95100 Catania, Italy; National Interuniversity Consortium for Materials Science and Technology (I.N.S.T.M.), Research Unit of Catania, 95125 Catania, Italy*

Valentina Greco − *Department of Chemical Sciences, University of Catania, 95100 Catania, Italy*

Valeria Buccilli − *Reparto Carabinieri Investigazioni Scientifiche Messina, 98122 Messina, Italy*

Pietro Maida − *Reparto Carabinieri Investigazioni Scientifiche Messina, 98122 Messina, Italy*

Davide Zavattaro − *Reparto Carabinieri Investigazioni Scientifiche Messina, 98122 Messina, Italy*

Gianfranco Sfuncia − *Consiglio Nazionale delle Ricerche, Istituto per la Microelettronica e Microsistemi, I-95121 Catania, Italy;* orcid.org/0000-0001-7355-7692

Giuseppe Nicotra − *Consiglio Nazionale delle Ricerche, Istituto per la Microelettronica e Microsistemi, I-95121 Catania, Italy*

Giuseppe Maccarrone − *Department of Chemical Sciences, University of Catania, 95100 Catania, Italy*

Antonino Gulino − *Department of Chemical Sciences, University of Catania, 95100 Catania, Italy; National Interuniversity Consortium for Materials Science and Technology (I.N.S.T.M.), Research Unit of Catania, 95125 Catania, Italy;* orcid.org/0000-0002-6850-3080

Complete contact information is available at: https://pubs.acs.org/10.1021/acsomega.2c02958

Author Contributions

Formal analysis: R.Santonocito, A.B.Carbonaro, V.Greco, G.Sfuncia; data curation: N.Tuccitto, A.Pappalardo and V.Cantaro; resources: G.Nicotra, V.Buccilli, P.Maida and D.Zavattaro; validation: G.Maccarrone, A.Gulino and A.Giuffrida; supervision and writing: A.Giuffrida and G.Trusso Sfrazzetto.

Funding

This research was funded by the University of Catania ["DetCWAs" (PIA.CE.RI 2020-2022-Linea Intervento 3), "NatI4Smart" PIA.CE.RI 2020-2022-Linea Intervento 2 and PIACERI with the project MAFmoF Materiali multifunzionali per dispositivi micro-optofluidici".

Notes

The authors declare no competing financial interest.

■ ACKNOWLEDGMENTS

The authors thank the University of Catania for the financial support and B.R.I.T. for the XPS facility.

■ REFERENCES

(1) Meyer, R.; Köhler, J.; Homburg, A.*Explosives*, 7th, completely revised and updated ed.; Wiley-VCH, 2016.

(2) Sun, S.; Wang, Y.; Lei, Y. Fluorescence based explosive detection: from mechanisms to sensory materials. *Chem. Soc. Rev.* **2015**, *44*, 8019−8061.
(3) Cruse, A. C.; Goodpaster, J. V. Optimization of gas chromatography/vacuum ultraviolet (GC/VUV) spectroscopy for explosive compounds and application to post-blast debris. *Forensic Chemistry* **2021**, *26*, 100362.
(4) Buryakov, I. A. Detection of explosives by ion mobility spectrometry. *J. Anal. Chem.* **2011**, *66*, 674−694.
(5) Bishwas, M. S.; Malik, M.; Poddar, P. Raman spectroscopy-based sensitive, fast and reversible vapour phase detection of explosives adsorbed on metal−organic frameworks UiO-67. *New J. Chem.* **2021**, *45*, 7145−7153.
(6) Wu, J.; Zhang, L.; Huang, F.; Ji, X.; Dai, H.; Wu, W. Surface enhanced Raman scattering substrate for the detection of explosives: Construction strategy and dimensional effect. *J. Hazard. Materials* **2020**, *387*, 121714.
(7) Ho, M. Y.; D'Souza, N.; Migliorato, P. Electrochemical Aptamer-Based Sandwich Assays for the Detection of Explosives. *Anal. Chem.* **2012**, *84*, 4245−4247.
(8) Rakow, N. A.; Suslick, K. S. A colorimetric sensor array for odour visualization. *Nature* **2000**, *406*, 710−713.
(9) Li, Z.; Askim, J. R.; Suslick, K. S. The Optoelectronic Nose: Colorimetric and Fluorometric Sensor Arrays. *Chem. Rev.* **2019**, *119*, 231−292.
(10) Babar, D. G.; Garje, S. S. Nitrogen and Phosphorus Co-Doped Carbon Dots for Selective Detection of Nitro Explosives. *ACS Omega* **2020**, *5*, 2710−2717.
(11) Qi, J.; Li, B.; Wang, X.; Fu, L.; Luo, L.; Chen, L. Rotational Paper-Based Microfluidic-Chip Device for Multiplexed and Simultaneous Fluorescence Detection of Phenolic Pollutants Based on a Molecular-Imprinting Technique. *Anal. Chem.* **2018**, *90*, 11827−11834.
(12) Li, Z.; Suslick, K. S. The Optoelectronic Nose. *Acc. Chem. Res.* **2021**, *54*, 950−960.
(13) Peveler, W. J.; Roldan, A.; Hollingsworth, N.; Porter, M. J.; Parkin, I. P. Multichannel Detection and Differentiation of Explosives with a Quantum Dot Array. *ACS Nano* **2016**, *10*, 1139−1146.
(14) Climent, E.; Biyikal, M.; Gröninger, D.; Weller, M. G.; Martínez-Máñez, R.; Rurack, K. Multiplexed Detection of Analytes on Single Test Strips with Antibody-Gated Indicator-Releasing Mesoporous Nanoparticles. *Angew. Chem., Int. Ed.* **2020**, *59*, 23862−23869.
(15) Liu, Y.; Li, J.; Wang, G.; Zu, B.; Dou, X. One-Step Instantaneous Detection of Multiple Military and Improvised Explosives Facilitated by Colorimetric Reagent Design. *Anal. Chem.* **2020**, *92*, 13980−13988.
(16) Fan, Y. Z.; Tang, Q.; Liu, S. G.; Yang, Y. Z.; Ju, Y. G.; Xiao, N.; Luo, H. Q.; Li, N. B. A smartphone-integrated dual-mode nanosensor based on novel green-fluorescent carbon quantum dots for rapid and highly selective detection of 2,4,6-trinitrophenol and pH. *Appl. Surf. Sci.* **2019**, *492*, 550−557.
(17) Liu, C.; Zhang, W.; Zhao, Y.; Lin, C.; Zhou, K.; Li, Y.; Li, G. Urea-Functionalized Poly(ionic liquid) Photonic Spheres for Visual Identification of Explosives with a Smartphone. *ACS Appl. Mater. Interfaces* **2019**, *11*, 21078−21085.
(18) Tawfik, S. M.; Sharipov, M.; Kakhkhorov, S.; Elmasry, M. R.; Lee, Y. Multiple Emitting Amphiphilic Conjugated Polythiophenes-Coated CdTe QDs for Picogram Detection of Trinitrophenol Explosive and Application Using Chitosan Film and Paper-Based Sensor Coupled with Smartphone. *Adv. Sci.* **2019**, *6*, 1801467.
(19) Tang, N.; Mu, L.; Qu, H.; Wang, H.; Duan, X.; Reed, M. A. Smartphone-Enabled Colorimetric Trinitrotoluene Detection Using Amine-Trapped Polydimethylsiloxane Membranes. *ACS Appl. Mater. Interfaces* **2017**, *9*, 14445−14452.
(20) Salles, M. O.; Meloni, G. N.; de Araujo, W. R.; Paixao, T. R. L. C. Explosive colorimetric discrimination using a smartphone, paper device and chemometrical Approach. *Anal. Methods* **2014**, *6*, 2047−2052.
(21) Zhang, D.; Jiang, J.; Chen, J.; Zhang, Q.; Lu, Y.; Yao, Y.; Li, S.; Liu, G. L.; Liu, Q. Smartphone-based portable biosensing system using impedance measurement with printed electrodes for 2,4,6-trinitrotoluene (TNT) detection. *Biosensor Bioelect.* **2015**, *70*, 81−88.
(22) Giuffrida, M. L.; Rizzarelli, E.; Tomaselli, G. A.; Satriano, C.; Trusso Sfrazzetto, G. A novel fully water-soluble Cu(I) probe for fluorescence live cell imaging. *Chem. Commun.* **2014**, *50*, 9835−9838.
(23) Puglisi, R.; Pappalardo, A.; Gulino, A.; Trusso Sfrazzetto, G. Multitopic Supramolecular Detection of Chemical Warfare Agents by Fluorescent Sensors. *ACS Omega* **2019**, *4*, 7550−7555.
(24) Tuccitto, N.; Riela, L.; Zammataro, A.; Spitaleri, L.; Li-Destri, G.; Sfuncia, G.; Nicotra, G.; Pappalardo, A.; Capizzi, G.; Trusso Sfrazzetto, G. Functionalized Carbon Nanoparticle-Based Sensors for Chemical Warfare Agents. *ACS Appl. Nano Mater.* **2020**, *3*, 8182−8191.
(25) Baptista, F. R.; Belhout, S. A.; Giordani, S.; Quinn, S. J. Recent developments in carbon nanomaterial sensors. *Chem. Soc. Rev.* **2015**, *44*, 4433−4453.
(26) Ji, W.; Yu, J.; Cheng, J.; Fu, F.; Zhang, Z.; Li, B.; Chen, L.; Wang, X. Dual-Emissive Near-Infrared Carbon Dot-Based Ratiometric Fluorescence Sensor for Lysozyme. *ACS Appl. Nano Mater.* **2022**, *5*, 1656−1663.
(27) Wang, X.; Yu, J.; Ji, W.; Arabi, M.; Fu, L.; Li, B.; Chen, L. On−Off−On Fluorescent Chemosensors Based on N/P-Codoped Carbon Dots for Detection of Microcystin-LR. *ACS Appl. Nano Mater.* **2021**, *4*, 6852−6860.
(28) Trusso Sfrazzetto, G.; Millesi, S.; Pappalardo, A.; Tomaselli, G. A.; Ballistreri, F. P.; Toscano, R. M.; Fragalà, I.; Gulino, A. Agile Detection of Chemical Warfare Agents by Machine Vision: a Supramolecular Approach. *Chem.—Eur. J.* **2017**, *23*, 1576−1583.
(29) Sun, X.; Wang, Y.; Lei, Y. Fluorescence based explosive detection: from mechanisms to sensory materials. *Chem. Soc. Rev.* **2015**, *44*, 8019−8061.
(30) Pandya, A.; Goswami, H.; Lodha, A.; Menon, S. K. A novel nanoaggregationdetection technique of TNT using selective and ultrasensitive nanocurcuminas a probe. *Analyst* **2012**, *137*, 1771−1774.
(31) Tripathi, N.; Kumar, R.; Singh, P.; Kumar, S. Ratiometric fluorescence "Turn On" probe for fast and selectivedetection of TNT in solution, solid and vapour. *Sens. Actuators B* **2017**, *246*, 1001−1010.
(32) Schindelin, J.; Arganda-Carreras, I.; Frise, E.; Kaynig, V.; Longair, M.; Pietzsch, T.; Preibisch, S.; Rueden, C.; Saalfeld, S.; Schmid, B.; Tinevez, J.-Y.; White, D. J.; Hartenstein, V.; Eliceiri, K.; Tomancak, P.; Cardona, A. Fiji: an open-source platform for biological-image analysis. *Nat. Methods* **2012**, *9*, 676−682.
(33) Hossein Keshaavaraz, M. Simple correlation for predicting detonation velocity of ideal and non-ideal explosives. *J. Hazard. Mater.* **2009**, *166*, 762−769.
(34) Zapata, F.; García-Ruiz, A. Determination of Nanogram Microparticles from Explosives after Real Open-Air Explosions by Confocal Raman Microscopy. *Anal. Chem.* **2016**, *88*, 6726−6723.
(35) Thurman, J. T.*Practical Bomb Scene Investigation*; Taylor & Francis: Boca Raton, FL, 2006.
(36) Christen, H. T.; Maniscalco, P. M.Weapons of mass effect-explosives. In *Homeland Security: Principles and Practice of Terrorism Response*; Maniscalco, P. M., Christen, H. T., Eds.; Jones and Bartlett Publishers: Sudbury, MA, 2011; pp 161−170.
(37) Gao, R.; Li, D.; Zhang, Q.; Zheng, S.; Ren, X.; Deng, W. GNPs-QDs core−satellites assembly: trimodal platform for on-site identification and detection of TNT in complex media. *Sens. Act. B: Chemical* **2021**, *328*, 128960.
(38) Xu, S.; Lu, H.; Li, J.; Song, X.; Wang, A.; Chen, L.; Han, S. Dummy Molecularly Imprinted Polymers-Capped CdTe Quantum Dots for the Fluorescent Sensing of 2,4,6-Trinitrotoluene. *ACS Appl. Mater. Interfaces* **2013**, *5*, 8146−8154.
(39) Tu, R.; Liu, B.; Wang, Z.; Gao, D.; Wang, F.; Fang, Q.; Zhang, Z. Amine-Capped ZnS-Mn^{2+} Nanocrystals for Fluorescence Detection of Trace TNT Explosive. *Anal. Chem.* **2008**, *80*, 3458−3465.

https://doi.org/10.1021/acsomega.2c02958
ACS Omega 2022, 7, 37122−37132

(40) Zou, W.-S.; Sheng, D.; Ge, X.; Qiao, J.-Q.; Lian, H.-Z. Room-Temperature Phosphorescence Chemosensor and Rayleigh Scattering Chemodosimeter Dual-Recognition Probe for 2,4,6-Trinitrotoluene Based on Manganese-Doped ZnS Quantum Dots. *Anal. Chem.* **2011**, *83*, 30−37.
(41) Liu, Y.; Zhou, Q.; Wu, Y.; Li, S.; Sun, S.; Sheng, X.; Zhan, Y.; Zhao, J.; Guo, J.; Zhou, B. Sensitive detection of 2,4,6-trinitrotoluene utilizing fluorescent sensor from carbon dots and reusable magnetic core-shell nanomaterial. *Talanta* **2021**, *233*, 122498.
(42) Tuccitto, N.; Catania, G.; Pappalardo, A.; Trusso Sfrazzetto, G. Agile Detection of Chemical Warfare Agents by Machine Vision: a Supramolecular Approach. *Chem.—Eur. J.* **2021**, *27*, 13715−13718.
(43) Li-Destri, G.; Fichera, L.; Zammataro, A.; Trusso Sfrazzetto, G.; Tuccitto, N. Self-assembled carbon nanoparticles as messengers for artificial chemical communication. *Nanoscale* **2019**, *11*, 14203−14209.

https://doi.org/10.1021/acsomega.2c02958
ACS Omega 2022, 7, 37122−37132